Composites Communications 21 (2020) 100403

Contents lists available at ScienceDirect

Composites Communications

journal homepage: www.elsevier.com/locate/coco

# A double-layered composite for lightning strike protection via conductive and thermal protection

Qianshan Xia [a], Zhichun Zhang [a], Hao Mei [a], Yanju Liu [b], Jinsong Leng [a,*]

[a] Center for Composite Materials and Structures, No. 2 YiKuang Street, Science Park of Harbin Institute of Technology (HIT), Harbin, 150080, PR China
[b] Department of Aerospace Science and Mechanics, No. 92 West DaZhi Street, Harbin Institute of Technology (HIT), Harbin, 150001, PR China

ARTICLE INFO

*Keywords:*
Buckypaper
Carbon fiber reinforced polymer
Lightning strike protection

ABSTRACT

This paper reports the fabrication and characterization of a novel silver modified buckypaper-carbon fiber/phenol-formaldehyde (SMBP-CF/PF) composite for lightning strike protection (LSP). The composite not only provides electrical protection with the SMBP, but also effectively reduces the lightning strike (LS) damage with the CF/PF layer for thermal dissipation. Residual strength rate of the SMBP-CF/PF-CFRP composite maintains 97.25% after the LS test. Compared with commercial materials, the usage of the SMBP-CF/PF composite demonstrates weight-reduced as well as the excellent LSP performance. Therefore, the lightweight SMBP-CF/PF composite can be applied as the novel LSP material for aircraft.

## 1. Introduction

Recent years, carbon fiber reinforced polymer (CFRP) composites have been widely applied in the aircraft industry and the usage rate of CFRP composite of advanced aircraft increased constantly, owing to low density and excellent mechanical property [1,2]. Compared with traditional metallic materials, CFRP composites used in the aircraft can reduce fuel consumption and improve fatigue resistance. However, CFRP aircraft may suffer fatal lightning strike (LS) damage, owing to poor conductivity [3]. Lightning generates huge Joule heat at the lightning attachment point, and the surface temperature increases to 3000–30000 °C [4,5]. It will cause catastrophic failure to CFRP structures [6–8].

Traditional lightning strike protection (LSP) method is introducing highly conductive metal mesh [9] or foil [10]. Due to high density, addition of metallic materials will increase the weight of the aircraft, and cause fuel consumption increasing. To overcome the drawbacks, lightweight carbon materials attract attentions from researchers [11,12], such as carbon nanofibers [8,12], carbon nanotubes (CNTs) [13,14], graphene [15,16] and buckypaper (BP) [17]. However, the LSP efficiency of these carbon materials is not enough. Even if metallic material can provide good electrical protection, LS still damages the CFRP matrix. For instance, Rajesh et al. [18], fabricated the CFRP composite protected by the Ag coating. After applying a LS current of 40 kA, damage area of the composite was 1886 $mm^2$ and damage depth is 0.75 mm. The reason is that the huge LS current causes serious thermal damage of the CFRP matrix. Whereas, few researchers pay attention to the material for thermal protection. The phenol-formaldehyde (PF) resin with excellent ablation resistance, high interlaminar shear strength and other advantages has been required by the aerospace industries as the thermal protection materials [19].

In this study, a silver modified buckypaper (SMBP)-carbon fiber/phenol-formaldehyde (CF/PF) composite was added onto the CFRP matrix surface through hot pressing to respectively serve as the conductive layer and the heating dissipating layer. According to characterization and analysis, the possible LSP mechanism of the SMBP-CF/PF protective structure was discussed in this work.

## 2. Materials and methods

To improve electrical conductivity, the buckypaper was modified by silver with good chemical inertness [20,21], according to previous report [22]. During the electrophoretic deposition (EPD) process, the applied DC voltage was 5 V and the deposition time was 240 s. The fabrication process of CF/PF prepreg was shown in Fig. S1 and the detailed descriptions about preparation are provided in the supporting information. After fully soaked, CF fabric impregnated PF was degasified and heated 6 h at 75 °C, to remove air bubbles and solvent. The mold was put into a freezer for easily demolding. 31 and 32 layers of CFRP prepregs were paved together and the stacking sequence was

* Corresponding author.
*E-mail address:* lengjs@hit.edu.cn (J. Leng).

https://doi.org/10.1016/j.coco.2020.100403
Received 4 June 2020; Received in revised form 12 June 2020; Accepted 14 June 2020
Available online 22 June 2020

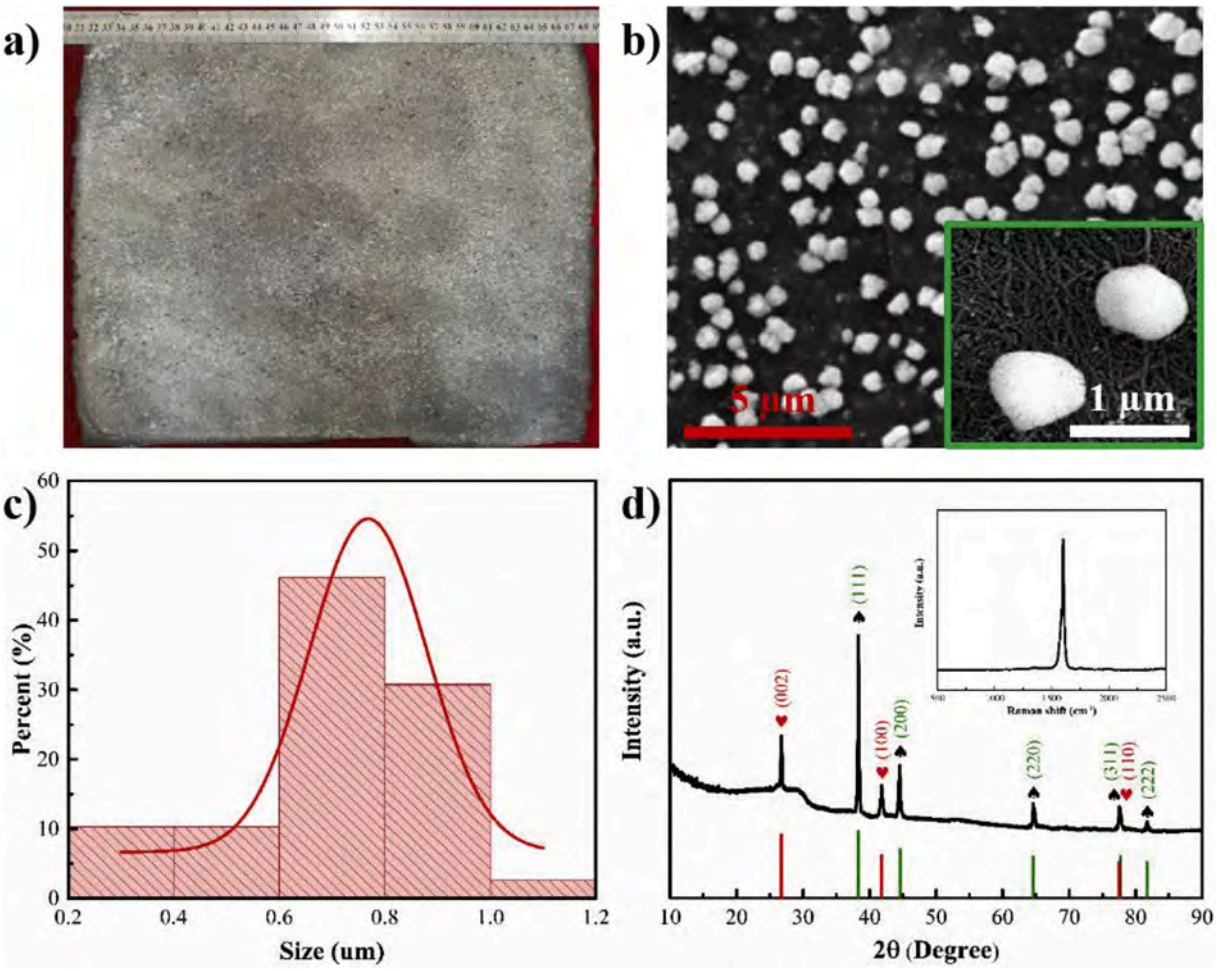


**Fig. 1.** a) Photo of the SMBP, b) SEM image of the SMBP, the inset is high magnification image, c) Particle diameter distribution of Ag particles in Fig. 1b, d) XRD pattern of the SMBP, the inset is its Raman spectrum.

$[0°/90°]_{16S}$, to form CFRP laminates. For fabricating Cu mesh/carbon fiber reinforced polymer (Cu/CFRP) and SMBP/CFRP specimens, Cu mesh and SMBP were placed on outmost layers of two CFRP laminates, respectively. The schematic profile of preform fabrication of SMBP-CF/PF-CFRP laminate was shown in Fig. S2a and the detailed descriptions of the preparation are provided in the supporting information. Its CFRP laminate contained 31 layers of prepregs. Subsequently, all four laminates were cured as shown in Fig. S2b.

Photo of the sample was obtained from a digital camera (Sony, ILCE-6000L). Morphology of the specimen was observed through a scanning electron microscope (SEM, VEGA3). The profile of the composite panel was displayed with two digital microscopes (VH-Z500R and SZX2-FOF). Damage area and depth of the sample were studied by a C-scan inspection device (Tecnatom, Composite IX) and a B-scan inspection device (Omni Scan MX), respectively. Temperature field variation of the sample was recorded with an infrared camera (FLIR A655sc). According to ASTM 7137, compressive strength of the sample was characterized by the AG-1 Material Testing Machine. According to SAE ARP 5412, all composite panels were subjected to current of DBC* combined waveform of the LS Zone 2A. Position of the sample in the setup and the test process were shown in Fig. S3 and Video S1. Detailed parameters of D, B and C* current waveforms were listed in Table S1, respectively. During the LS process, the electrical charge (Q) represents the total energy of the impulse current and can be expressed as Equation (1). The action integral (AI) as the specific energy can be written as Equation (2).

Supplementary video related to this article can be found at https://doi.org/10.1016/j.coco.2020.100403

## 3. Results and discussion

As presented in Fig. 1a, the SMBP has uniformly metallic luster and possesses sufficient flexibility for manufacturing the CFRP component with complex shape. As displayed in Fig. 1b, spherical silver (Ag) particles with uniform diameters discretely attach on the CNT network. The Ag particles do not fill in holes of CNT networks. The SMBP still maintains channels for resin penetrating. Size distribution of the Ag particle is ranged from 0.2 to 1.2 μm as displayed in Fig. 1c and its maximum content of particle diameter locates in the range from 700 to 900 nm. It indicates the EPD method is useful for obtaining uniform SMBP. X-ray diffraction (XRD) pattern of the SMBP is shown in Fig. 1d. Three typical characteristic peaks of CNTs appear at 26.7°, 41.8° and 77.7° (red heart signs), which correspond to (002), (100) and (110) facets of graphitic structure (PDF#26–1079) [23], respectively. In addition, the SMBP contains another five distinct diffraction peaks, which appear at 38.3°, 44.6°, 64.6°, 77.5° and 82°. The five peaks attribute to (111), (200), (220), (311) and (222) facets (black spade signs) of the elemental silver (PDF#65–2871), respectively. It proves that almost all of Ag particles are elemental. As displayed in the inset, $I_D/I_G$ value of the SMBP is only 0.024, and $I_D/I_G$ value of the BP is 0.023 (Fig. S4). The tiny difference illustrates the EPD process generates few defects and does not affect intrinsic properties of CNTs. Electrical conductivity is a crucial property for the LSP material. Electrical conductivities of BP and SMBP are 525.11 S/cm and 5091.65 S/cm, respectively. It indicates that EPD technology is a feasible strategy to improve the electrical conductivity.

Pore diameter distribution of the SMBP and contact angles of epoxy

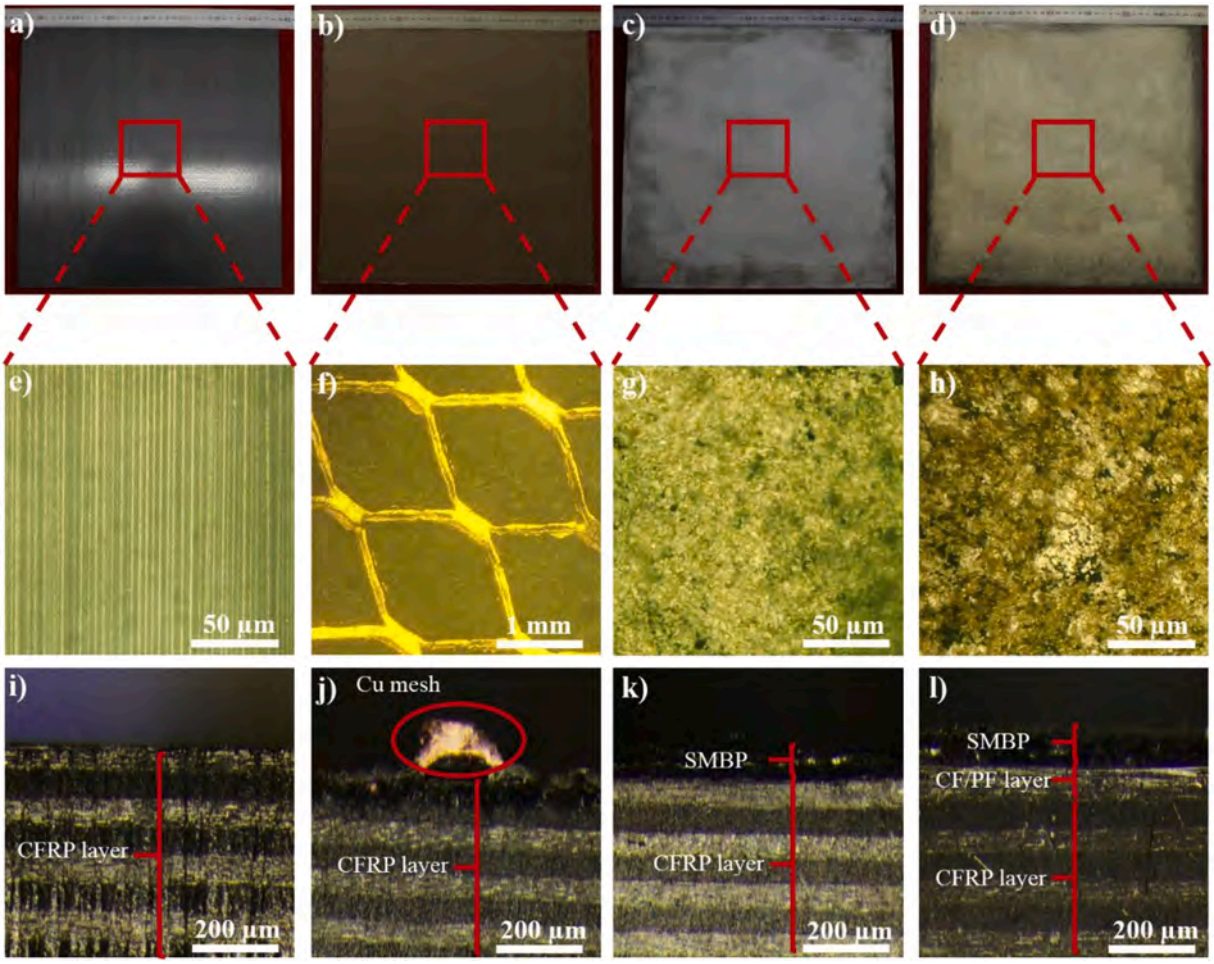


**Fig. 2.** Photos of a) CFRP panel, b) Cu/CFRP panel, c) SMBP/CFRP panel and d) SMBP-CF/PF-CFRP panel, e)-h) surface morphologies corresponding to a)-d), i)-l) morphologies of cross sections corresponding to a)-d).

and PF resin droplets on the SMBP are displayed in Fig. S5, and the detailed descriptions can be found in the supporting information. According to the International Union of Pure and Applied Chemistry's classification [24], the SMBP can be considered as a typical mesoporous material. Contact angles of epoxy and PF resin droplets on two sides of SMBP were observed, for evaluating their spreading abilities. All contact angles of epoxy and PF droplets on the SMBP at room temperature are less than 30°. It illustrates that both the two resins can easily spread on two sides of the SMBP. SMBP can be permeated by the rich epoxy and PF resins to form the stable composite. Pyrolysis processes of SMBP and CF/PF are shown in Fig. S6 and detailed descriptions is in the supporting information. Ag content of the SMBP is about 25.22%, according to Fig. S6a and b. It indicates that the SMBP still possesses light weight. As shown in Fig. S6c, the CF/PF composite starts to degrade at 118 °C, due to volatilization of residual curing agents and raw materials without reaction. The pyrolysis of PF resin starts at 319 °C, CF starts to pyrolyze at 640 °C and ends at 806 °C [25].

Macro and micro morphologies of composite panels were characterized. Photos of CFRP, Cu/CFRP, SMBP/CFRP panel and SMBP-CF/PF-CFRP panel are shown in Fig. 2a, b, c and d, respectively. Sizes of all the composite panels are 360 × 360 $mm^2$. Smooth surface of SMBP-CF/PF-CFRP panel illustrates porous structure and good resin wettability of the SMBP is beneficial to resin penetration. CF monofilaments of the CFRP composite are well-arranged after curing (Fig. 2e). The golden mesh is Cu mesh of the Cu/CFRP composite and its long pitch is about 3 mm (Fig. 2f). White light-spots in Fig. 2g and h are Ag particles uniformly attaching on SMBP surfaces. Most of particles are not divorced from SMBP surfaces. However, surface color of the SMBP-CF/PF-CFRP composite is darker than the SMBP/CFRP composite, owing to the PF penetration. It can be found that the layout of CF monofilaments is orthogonal and CFRP layers stack compactly Fig. 2i. Fig. 2j displays that diameter of the single Cu wire is about 80 μm. The bottom of the Cu wire attaches on the matrix surface and the Cu mesh is not filled by enough resin. The SMBP is embedded compactly on the top surface of the composite and its surface is covered by enough resin (Fig. 2k). Its thickness is about 70 μm. Thicknesses of SMBP and CF/PF layers are about 70 and 150 μm, respectively (Fig. 2l). The SMBP is covered by PF resin. The SMBP-CF/PF protective structure compactly adhered on the CFRP matrix is difficult to break away under high pressure impact caused by the LS. The stable structure will play a significant role in maintaining the LSP performance.

For studying protective performance, aforementioned four composite panels underwent simulated LS tests. Fig. 3a–h show macro and micro morphologies of above four composite panels after LS tests. As shown in Fig. 3a and e, LS damage of the CFRP panel is very serious, and some CFs locating the deep depth fracture. There are Cu mesh exfoliating, resin losing and CFs cracking in the damage zone (Fig. 3b and f). In the LS zone, only a few CFs of the SMBP/CFRP panel crack (Fig. 3c and g). The surface glossiness of the composite reduces owing to the epoxy resin decomposing. As shown in Fig. 3d and h, there are small areas of SMBP and PF resin of the CF/PF surface losing. It is worth noting that CF fabric of the CF/PF layer is almost intact. Fig. 3i–l are C scan images corresponding to Fig. 3a–d, respectively. The undamaged zone is shown as red and the color changing from red to black stands for damage

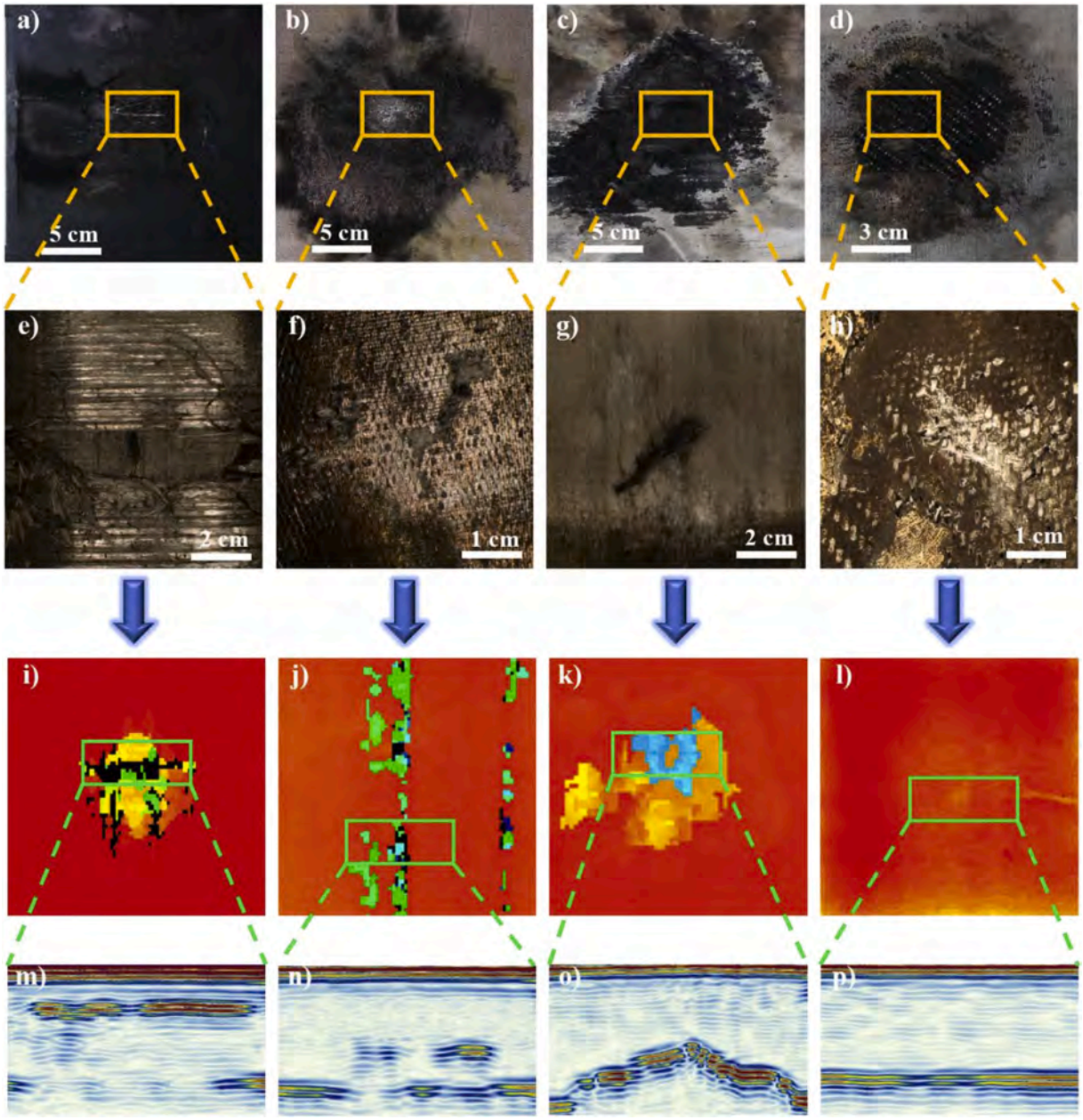


**Fig. 3.** Damage areas of a) CFRP panel, b) Cu/CFRP panel, c) SMBP/CFRP panel and d) SMBP-CF/PF-CFRP panel after LS tests, e)-h) micrographs of composite panels corresponding to a)-d), i)-l) and m)-p) C and B scan images of composite panels corresponding to a)-d).

depth deepening. The damaged depth as a significant parameter can directly affect the residual strength of CFRP composite after the LS. Specimens were detected by the B scan inspection to identify damage depths. B-scan zones of samples are marked with green squares in corresponding to their C scan images. Fig. 3i and m illustrate that the damage area of the CFRP panel is 113 × 104 $mm^2$ and its maximum damage depth is about 2.82 mm. Due to poor conductivity, great Joule heat generates in the LS zone, while the heat cannot be rapidly conducted along the surface and causes serious pyrolysis of the CFRP composite along the depth direction. Damage area of the Cu/CFRP panel is 173 × 178 $mm^2$ and its damage depth reaches 1.64 mm (Fig. 3j and m). It demonstrates that the Cu mesh with excellent conductivity can dissipate LS energy along the composite surface. The damage zones show the scattered distribution around the LS attachment point. Damage area and depth of the SMBP/CFRP panel are 165 × 155 $mm^2$ and 1.8 mm (Fig. 3k and o). The main damage focuses on the zone around the LS attachment point. The SMBP possesses the larger conductive area than the Cu mesh, which enhances conduction effectiveness for the LS energy. Damage area of the SMBP-CF/PF-CFRP panel is 125 × 94 $mm^2$ and the damage zone presents a circle (Fig. 3l). Fig. 3p shows the damage depth is only 0.14 mm. The LS only damages SMBP and CF/PF layer. It indicates that the SMBP-CF/PF composite as the LSP structure can effectively protect the CFRP matrix.

The performance of the LSP structure can be directly evaluated by residual strength of the composite after the LS. Residual strength values of the above-mentioned composite composites were obtained through compressive tests as shown in Fig. S7, and the detailed descriptions can be found in the supporting information. In contrast with other specimens, retention rate of compressive strength of the SMBP-CF/PF-CFRP composite is maximum (97.25%). SMBP-CF/PF protective structure displays excellent LSP performance. During the LS process, fuel tank, engine and other parts of the aircraft need strictly limiting the temperature variation, thus maximum temperatures of non LS sides of the LSP materials and thermal transmission process of the CF/PF layer were

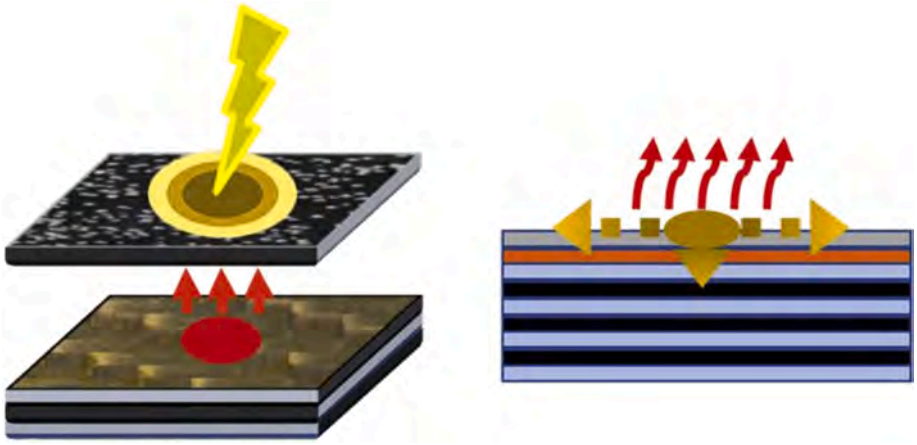

**Fig. 4.** Schematic diagram of the LSP mechanism of the SMBP-CF/PF composite.

studied as shown in Figs. S8 and S9, respectively. The detailed descriptions are in the supporting information [26]. During simulated LS tests, temperature difference of the non LS face of the SMBP-CF/PF-CFRP panel is only 44.9 °C and lower than other composite panels. It proves that the SMBP-CF/PF protective structure can effectively reduce the LS energy transferring to the CFRP matrix.

Schematic diagram of LSP mechanism of the SMBP-CF/PF composite is presented in Fig. 4. Yellow and red arrows stand for LS current conducting and Joule heat dissipating, respectively. At the initial stage, SMBP with high conductivity and large conduction area can effectively conduct LS current and reduce generation of Joule heat. Under high temperature, PF resin decomposes and absorbs heat via the enthalpy change reaction. The charring layer that generates from pyrolysis of the PF resin, possesses high radiation coefficient and can radiate part of the residual heat to the environment. Through the consumption, the CF/PF layer prevents the Joule heat from transferring into the matrix and reduces the heat damage depth. Therefore, the SMBP-CF/PF composite as a LSP structure can effectively reduce the damage of the CFRP matrix.

## 4. Conclusion

The SMBP-CF/PF-CFRP composite was prepared in this work for LSP. Compared with traditional LSP materials, the SMBP-CF/PF composite not only provides the electrical protection with the SMBP, but also protect the CFRP matrix from thermal damage with the CF/PF layer, to effectively reduce the LS damage. The compressive strength retention rate of the SMBP-CF/PF-CFRP composite reaches up to 97.25%, which is higher than the Cu/CFRP composite (96.09%). The temperature variation of the non LS side of the SMBP-CF/PF-CFRP composite (44.9 °C) is lower than the Cu/CFRP composite (51.1 °C). Especially, the SMBP-CF/PF used as the LSP structure can reduce about 50% of weight than the Cu mesh. Thus, the SMBP-CF/PF composite is a promising material to provide excellent LSP efficiency for the CFRP aircraft.

## Declaration of competing interest

The authors declare that they have no known competing financial interests or personal relationships that could have appeared to influence the work reported in this paper.

## CRediT authorship contribution statement

**Qianshan Xia:** Writing - original draft, Methodology. **Zhichun Zhang:** Methodology. **Hao Mei:** Investigation. **Yanju Liu:** Supervision, Validation. **Jinsong Leng:** Conceptualization, Writing - review & editing.

## Acknowledgement

This work is supported by the National Natural Science Foundation of China [Grant No.11632005].

## Appendix A. Supplementary data

Supplementary data to this article can be found online at https://doi.org/10.1016/j.coco.2020.100403.

## References

[1] S. Du, Advanced composite materials and aerospace engineering, Acta Mater. Compos. Sin. 24 (2007) 1–12, https://doi.org/10.13801/j.cnki.fhclxb.2007.01.001.
[2] M. Gagne, D. Therriault, Lightning strike protection of composites, Prog. Aero. Sci. 64 (2014) 1–16, https://doi.org/10.1016/j.paerosci.2013.07.002.
[3] A. Miller, K. Kollins, The Boeing 787 Dreamliner, 22nd American Society for Composites Technical Conference, Seattle, Washington State, 2007.
[4] L. Carporzen, B.P. Weiss, S.A. Gilder, A. Pommier, R.J. Hart, Lightning remagnetization of the Vredefort impact crater: No evidence for impact-generated magnetic fields, J. Geophys. Res.: Planets 117 (2012) E01007, https://doi.org/10.1029/2011je003919.
[5] Paria Naghipour, Evan J. Pineda, S.M. Arnold, Simulating Damage Due to a Lightning Strike Event: Effects of Temperature Dependent Properties on Interlaminar Damage, SIMULIA Community Conference, Providence RI, United States, 2014, pp. 1–15.
[6] Y. Hirano, S. Katsumata, Y. Iwahori, A. Todoroki, Artificial lightning testing on graphite/epoxy composite laminate, Compos. Part A Appl Sci. 41 (2010) 1461–1470, https://doi.org/10.1016/j.compositesa.2010.06.008.
[7] P. Feraboli, M. Miller, Damage resistance and tolerance of carbon/epoxy composite coupons subjected to simulated lightning strike, Compos. Part A Appl Sci. 40 (2009) 954–967, https://doi.org/10.1016/j.compositesa.2009.04.025.
[8] J.H. Gou, Y. Tang, F. Liang, Z.F. Zhao, D. Firsich, J. Fielding, Carbon nanofiber paper for lightning strike protection of composite materials, Compos. B Eng. 41 (2010) 192–198, https://doi.org/10.1016/j.compositesb.2009.06.009.
[9] F.A. Fisher, J. Plumer, Lightning Protection of Aircraft, NASA Reference Publication, 1977.
[10] R Winston Revie, H. Uhlig, Corrosion and Corrosion Control: an Introduction to Corrosion Science and Engineering, Wiley, 2008.
[11] J. Baur, E. Silverman, Challenges and opportunities in multifunctional nanocomposite structures for aerospace applications, MRS Bull. 32 (2007) 328–334, https://doi.org/10.1557/Mrs2007.231.
[12] B. Zhang, V.R. Patlolla, D. Chiao, D.K. Kalla, H. Misak, R. Asmatulu, Galvanic corrosion of Al/Cu meshes with carbon fibers and graphene and ITO-based nanocomposite coatings as alternative approaches for lightning strikes, Int. J. Adv. Manuf. Technol. 67 (2013) 1317–1323, https://doi.org/10.1007/s00170-012-4568-3.
[13] I.W. Chen, R. Liang, H. Zhao, B. Wang, C. Zhang, Highly conductive carbon nanotube buckypapers with improved doping stability via conjugational cross-linking, Nanotechnology 22 (2011) 485708, https://doi.org/10.1088/0957-4484/22/48/485708.
[14] J.H. Han, H. Zhang, M.J. Chen, D. Wang, Q. Liu, Q.L. Wu, et al., The combination of carbon nanotube buckypaper and insulating adhesive for lightning strike protection of the carbon fiber/epoxy laminates, Carbon 94 (2015) 101–113, https://doi.org/10.1016/j.carbon.2015.06.026.
[15] B. Wang, Y. Duan, Z. Xin, X. Yao, D. Abliz, G. Ziegmann, Fabrication of an enriched graphene surface protection of carbon fiber/epoxy composites for lightning strike

via a percolating-assisted resin film infusion method, Compos. Sci. Technol. 158 (2018) 51–60, https://doi.org/10.1016/j.compscitech.2018.01.047.
[16] L. Wang, X. Shi, J. Zhang, Y. Zhang, J. Gu, Lightweight and robust rGO/sugarcane derived hybrid carbon foams with outstanding EMI shielding performance, J. Mater. Sci. Technol. 52 (2020) 119–126, https://doi.org/10.1016/j.jmst.2020.03.029.
[17] S. Mall, B.L. Ouper, J.C. Fielding, Compression strength degradation of nanocomposites after lightning strike, J. Compos. Mater. 43 (2009) 2987–3001, https://doi.org/10.1177/0021998309345337.
[18] P.S.M. Rajesh, F. Sirois, D. Therriault, Damage response of composites coated with conducting materials subjected to emulated lightning strikes, Mater. Des. 139 (2018) 45–55, https://doi.org/10.1016/j.matdes.2017.10.017.
[19] J. Feng, J. Li, L. Chen, Y. Qin, X. Zhang, J. Gu, et al., Enhanced thermal stabilities and char yields of carbon fibers reinforced boron containing novolac phenolic resins composites, J. Polym. Res. 24 (2017), https://doi.org/10.1007/s10965-017-1338-9.
[20] C. Liang, P. Song, H. Qiu, Y. Zhang, X. Ma, F. Qi, et al., Constructing interconnected spherical hollow conductive networks in silver platelets/reduced graphene oxide foam/epoxy nanocomposites for superior electromagnetic interference shielding effectiveness, Nanoscale 11 (2019) 22590–22598, https://doi.org/10.1039/c9nr06022g.
[21] C. Liang, K. Ruan, Y. Zhang, J. Gu, Multifunctional flexible electromagnetic interference shielding silver nanowires/cellulose films with excellent thermal management and Joule heating performances, Acs Appl. Mater. Interfaces 12 (2020) 18023–18031, https://doi.org/10.1021/acsami.0c04482.
[22] Q. Xia, H. Mei, Z. Zhang, Y. Liu, Y. Liu, J. Leng, Fabrication of the silver modified carbon nanotube film/carbon fiber reinforced polymer composite for the lightning strike protection application, Compos. B Eng. 180 (2020) 107563, https://doi.org/10.1016/j.compositesb.2019.107563.
[23] H. Chu, Q. Xia, Z. Zhang, Y. Liu, J. Leng, Sesame-cookie topography silver nanoparticles modified carbon nanotube paper for enhancing lightning strike protection, Carbon 143 (2019) 204–214, https://doi.org/10.1016/j.carbon.2018.11.022.
[24] H. Hu, X. Lu, F. Wang, J. He, J. Li, M. Fan, Activated Carbon Based Selective Purification of Medical Grade NO Starting from Arc Discharge Method, Carbon, 2011, pp. 2197–2205, https://doi.org/10.1016/j.carbon.2011.01.046.
[25] Y. Xu, Y. Yang, Y. Zhang, Z. Wang, Pyrolysis characteristics of unidirectional carbon fiber/epoxy prepreg, Acta Mater. Compos. Sin. 35 (2018) 2442–2448, https://doi.org/10.13801/j.cnki.fhclxb.20171208.004.
[26] W. Li, J. Zhang, G. Fang, W. Li, J. Liang, S. Meng, Evaluation of numerical ablation model for charring composites, Sci. China Technol. Sci. 62 (2019) 1322–1330, https://doi.org/10.1007/s11431-018-9476-2.